Available online at www.sciencedirect.com
SCIENCE DIRECT®
Pergamon
Acta Materialia 51 (2003) 1283–1291
Acta MATERIALIA
www.actamat-journals.com

Measurement of the strains induced upon thermal oxidation of an alumina-forming alloy

K.-J. Kang [a,*], J.W. Hutchinson [b], A.G. Evans [c]

[a] *Department of Mechanical Engineering, Chonnam National University, Kwangju, 500-757, South Korea*
[b] *Division of Engineering and Applied Sciences, Harvard University, Cambridge, MA 02138, USA*
[c] *Materials Department, University of California , Santa Barbara, CA 93106-5050, USA*

Received 24 September 2002; accepted 31 October 2002

Abstract

The mechanisms that govern the formation of a thermally grown alumina on Al-containing super-alloys has been the subject of much recent speculation, because of the key influence of this oxide on the durability of thermal barrier systems for gas turbines. Among the important issues to be resolved are the location of the new oxide growth (interface, surface or internal grain boundary), the strains induced by the growth on non-planar surfaces and the associated stresses. To address some of the uncertainties, an experimental probe is designed. The experiments are based on the curvature changes, $\Delta\kappa$, that occur on curved thin foils, caused by differences in strain accommodation on convex and concave surfaces. Experiments performed on thin FeCrAlY foils provide a vivid illustration of the strains induced upon growth, demonstrating a large increase in the radius of curvature upon oxidation. The sign and magnitude of the changes affirm that most of the new oxide forms at the interface.

Keywords: Thermal barrier coatings; Oxidation; Thermally grown oxides; Growth stresses

1. Introduction

Multi-layer thermal barrier systems are now commonly used in gas turbines [1–3]. They comprise a single crystal Ni alloy substrate, an intermediate Ni(Al) alloy layer (the bond coat) that acts as a barrier to oxidation and an outer layer, typically yttria-stabilized zirconia, that provides the thermal insulation. A thermally grown oxide (TGO), generally α–Al_2O_3, forms between these two layers upon exposure to oxygen at high temperature [1–11]. The presence of the TGO often dominates the performance and durability of the system. That is, as the TGO layer thickens, the stresses induced in this layer, as the system thermally cycles, interact with the surrounding material to instigate failure mechanisms. Several such mechanisms have been described [1–4,7–10].

There are two sources of stress in the TGO: both nominally compressive [1,4,6,11]. One is governed by the thermal expansion misfit with the substrate. It has been comprehensively characterized by piezo-spectroscopy and X-ray measurements [11–

* Corresponding author. Tel.: +82-625-301668; fax: +82-625-301689.
E-mail address: kjkang@chonnam.ac.kr (K.-J. Kang).

1359-6454/03/$30.00
doi:10.1016/S1359-6454(02)00523-2

14]. The other, associated with strains induced upon growth of the TGO, has only recently been subject to a fundamental assessment [15]. This strain is the source of growth related displacements and stresses. When the oxide forms, it occupies a larger volume than the original alloy. The ratio of the volume of the oxide to the alloy consumed, *m*, is a basic parameter [1,16–19]. It is related to (but not the same as) the Pilling–Bedworth ratio [19]. It will be estimated experimentally in this study.

For typical bond coats, most of the new oxide has been surmised to form at the interface, as oxygen anion ingress along the TGO grain boundaries encounters the Al in the alloy, resulting in thickening of the TGO [1–3,15,20] (Fig. 1). Some of the oxide also forms on grain boundaries internal to the TGO, presumably due to a counter flux of Al cations and O anions [15,20,22]. New measurement protocols are needed to guide further understanding. The present article describes a method capable of determining where the new TGO forms. The method originates with two prior explorations: (a) an analysis of the displacement of curved, thin foils upon oxidation [16] and (b) a series of measurements involving α–Al_2O_3 formation on thin, flat foils of FeCrAlY [20]. On curved surfaces, the sign of the stresses induced as the TGO grows depends on the predominant formation site for the new oxide, as well as whether the surface is concave or convex. The consequence is that a thin ribbon of curved bond coat material develops a bending moment as it oxidizes, causing the curvature to change [16,21]. The sign of the curvature change (positive or negative), and its magnitude, are sensitive to the growth site. Based on these concepts, an experimental approach is devised, based primarily on the U-configuration depicted on Fig. 2. Measurements are performed on ribbons of FeCrAlY, which oxidizes to form α–Al_2O_3, with the new oxide believed to form predominantly at the interface [1,15,20,22].

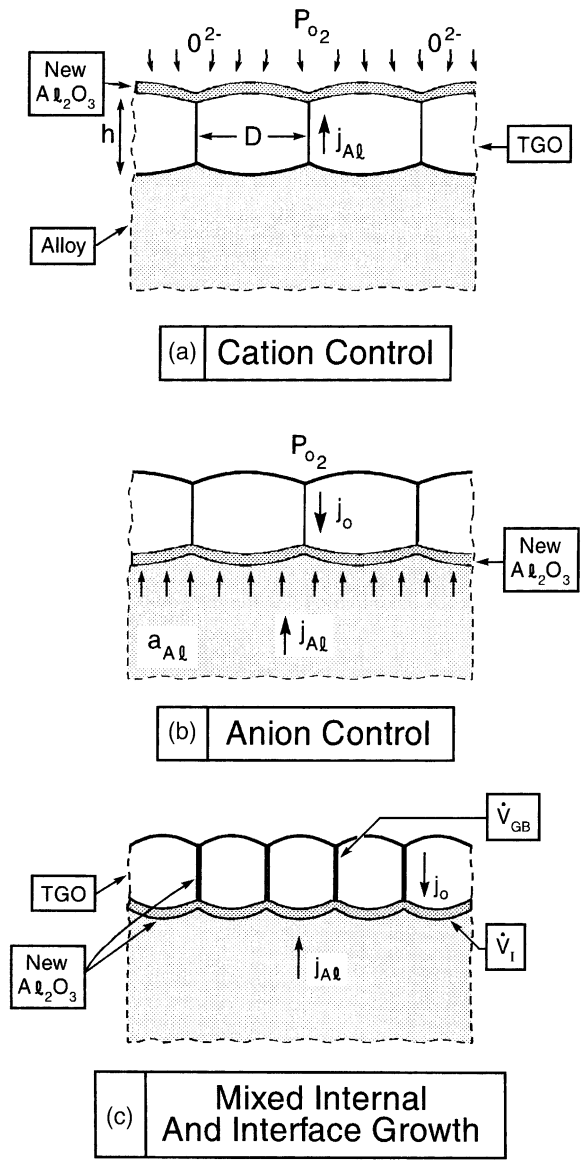

Fig. 1. Schematic of the growth of oxide layers under: (a) cation-diffusion controlled and (b) anion-diffusion controlled conditions, showing the ion fluxes and diffusion paths. In both cases, oxide growth occurs normal to the metal/oxide interface. (c) Mixed internal and interface formation of new oxide. The dimensions used in Appendix A are also shown.

2. Basic concepts

For *anion-controlled* oxide growth, on a *convex* surface, the alloy beneath the interface is replaced by an oxide with a larger radial dimension [1,15,21]. For displacement compatibility, the oxide must expand radially by placing it in *tangential tension*, combined with a small radial compression [16]. For a *concave* surface, the corresponding growth requires that the oxide contract

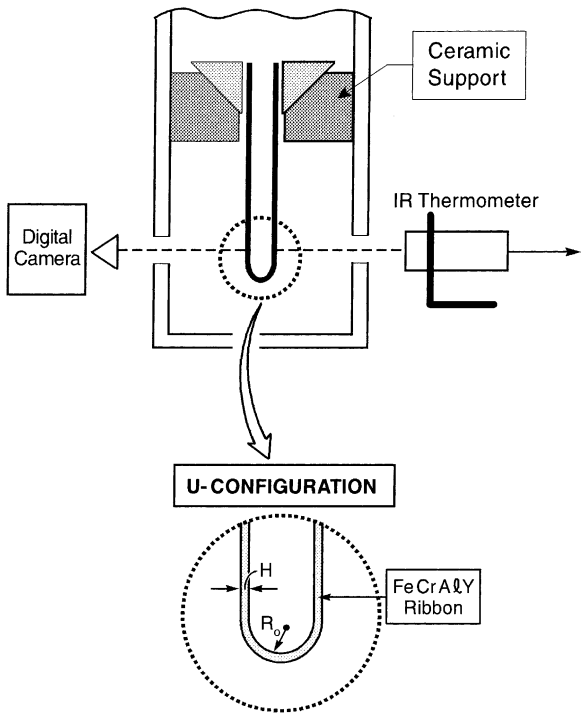

Fig. 2. Schematic of the test methodology based on a U-shaped specimen.

radially, causing it to be in *tangential compression.* The converse effects occur for *cation-controlled* growth [16]. Accordingly, the TGO experiences growth stresses of opposite sign on concave and convex surfaces and, moreover, the signs are inverted for the anion and cation controlled cases. These signs remain unchanged when the configuration becomes a curved thin ribbon (Fig. 2), although the magnitudes are altered. Because the stresses in the TGO have opposite signs on the opposing surfaces, they impose a bending moment that causes the curvature to change. For *anion-control*, since the concave surface is in compression and vice versa, the moment acts *outward* and the radius of curvature, *R*, *increases*. Conversely, for *cation-control*, the inward acting moment causes *R* to decrease. The experiments are performed on FeCrAlY foils. To facilitate interpretation, the foil thickness and test temperature have been chosen to assure that the stresses in the FeCrAlY are relaxed by creep, while the TGO remains essentially elastic. Based on the extensive assessment by Tolpygo and Clarke [11,22], this criterion appears to be satisfied for foils having thickness, $H \leq 160$ μm, and a test temperature about 1200 °C.

3. Experimental protocol

3.1. Experimental procedures

The as-received alloy foils, which were in the as-rolled state, were cut into ribbons and the edges polished. They were annealed at 800 °C for 10 min to equilibrate the microstructure, then mechanically polished to optical flatness using 3 μm diamond paste and cleaned in acetone. Subsequently, they were deformed around a 4 mm diameter mandrel to create a U by tensile loading to 250 N in a servo-hydraulic machine, through a friction grip, at a displacement rate of 1 μm/s. They were degreased in acetone and annealed at 420 °C for 12 h to remove the residual stress. The U-shaped foils were clamped into a ceramic fixture within a resistance furnace (Fig. 2). Tests were conducted at 1200 °C. The maximum width, δ_{max}, was measured as a function of the exposure time, by using an optical telescope. The mass of the specimens was determined before and after each test.

Once the tests had been completed, the oxidized ribbons were sectioned using a focused ion beam (FIB) system to avert the edge rounding that occurs upon mechanical grinding and polishing. The thickness of the TGO was measured and recorded.

4. Measurements and observations

4.1. Volumetric strain

The experiments were conducted on 90 μm thick FeCrAlY foils in the U-configuration. The TGO thickness, *h*, was measured on specimens subjected to a range of exposure times by creating FIB sections and imaging. The results revealed a thickening (Fig. 3) that deviates slightly from parabolic. The thickness is found to be the same on both the concave and convex sides. A plot of the mass change against the measured TGO thickness

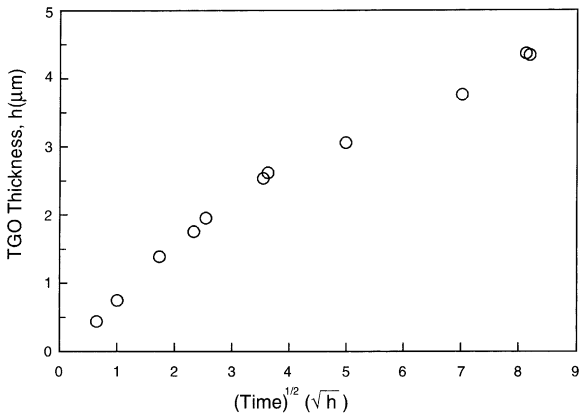

Fig. 3. Plot of TGO thickness as a function of exposure time: The square root of time ($\sqrt{h}$) is used as the abscissa to assess the suitability of the parabolic rate approximation.

obtained on the same specimens (Fig. 4) indicates the expected linearity.

The same sections were used to measure the change in the overall thickness of the foils, $H-H_0$, plotted against the total TGO thickness, $2h$, on Fig. 5. From geometry, the slope of this plot, $\lambda = (H - H_0)/2h$, is related to the normal component of the stress-free strain upon oxidation (Appendix A). Moreover, since the fraction of the new oxide created at the interface appreciably exceeds that formed on the internal grain boundaries [15], this measurement provides an estimate of the volumetric strain:

$$m \approx [1-\lambda]^{-1} \approx 2.2 \quad (1)$$

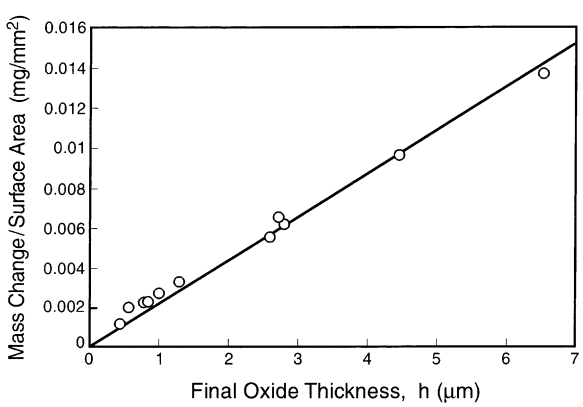

Fig. 4. Correlation between change in mass per unit area and the TGO thickness.

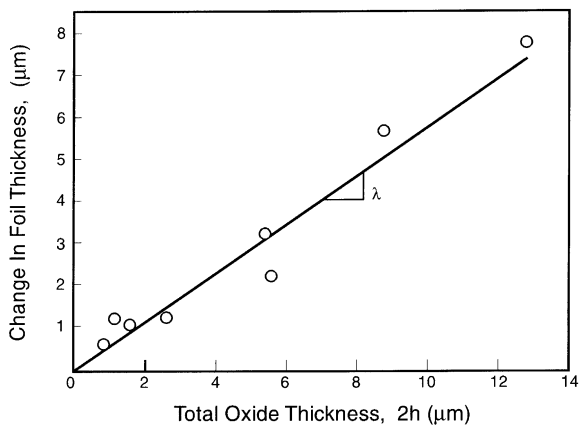

Fig. 5. Change in the ribbon thickness as a function of total TGO thickness.

This strain is larger than the Pilling–Bedworth ratio for conversion of Al→α–Al_2O_3 [19], presumably because of the small reduction in the β–FeCrAlY lattice constant as Al is removed.

4.2. U-configuration

In situ optical images taken of the FeCrAlY foils at the beginning and the end of an isothermal exposure are shown in Fig. 6. The outward deflections caused by TGO growth are illustrated. The sign of the change immediately indicates that the new oxide forms primarily at the alloy/oxide interface. Such images were used to measure the displacement at the location of the maximum, δ_{max}. Results for five of the tests are summarized in Fig. 7(a). While there is evident variability between specimens, the trend appears to be systematic. After subjecting such specimens to various exposures, FIB sections were used to measure the TGO thickness. This procedure allows determination of the relationship between δ_{max} and h, as plotted on Fig. 7(b). This result provides the basis for a comparison with theory, upon superposing predicted curves onto the figure.

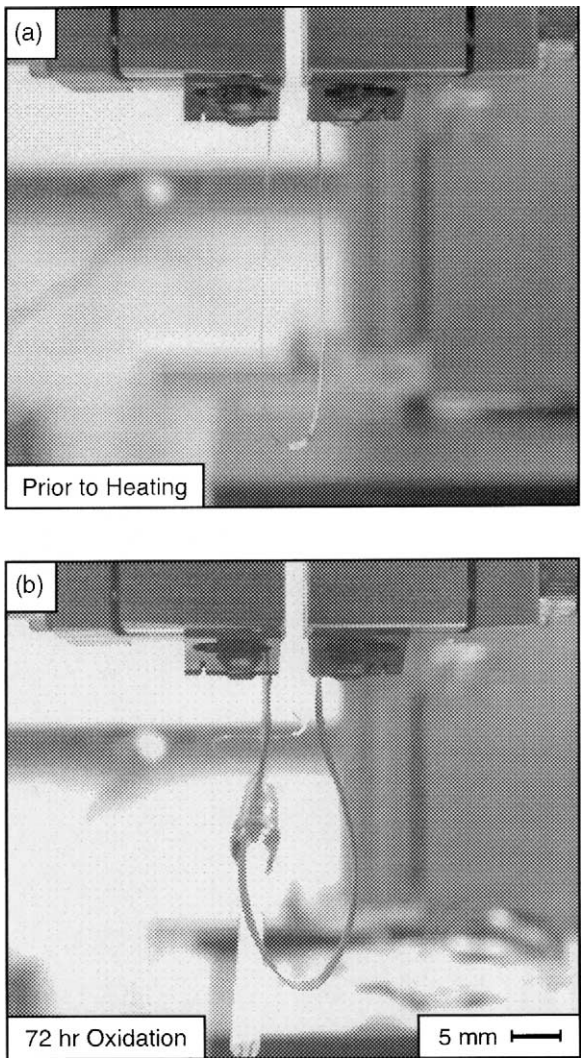

Fig. 6. Images obtained before and after isothermal oxidation, showing the change in the shape of the U-geometry.

5. Deflection analysis

5.1. Constant curvature segment

The U-specimen is analyzed by first imagining that the curved segment is detached from the straight sides and its curvature change determined as a function of the growing oxide. This segment drives the deformation of the entire U-specimen (Fig. 8). The re-attachment is addressed in the subsequent section. A detached segment of constant

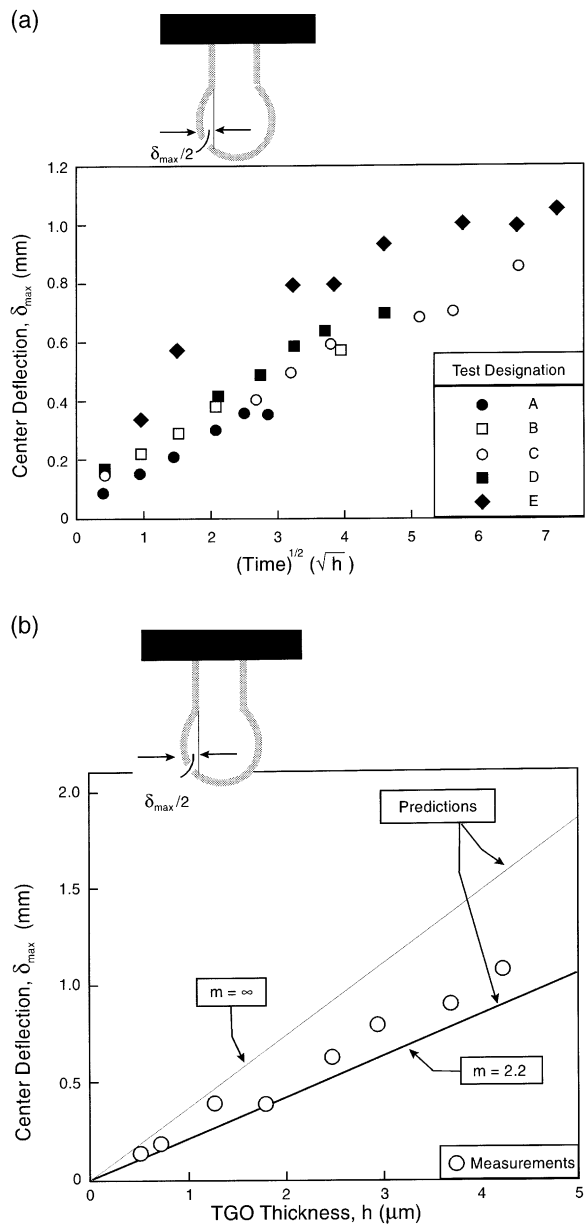

Fig. 7. (a) Changes in the maximum deflection of the U with time measured on five different specimens (designated A–E) using $\sqrt{h}$ the abscissa (see Fig. 3). (b) Variation in the maximum deflection with the TGO thickness measured on eight separate specimens. Theoretical results are superposed for two choices of the volume expansion parameter, *m*.

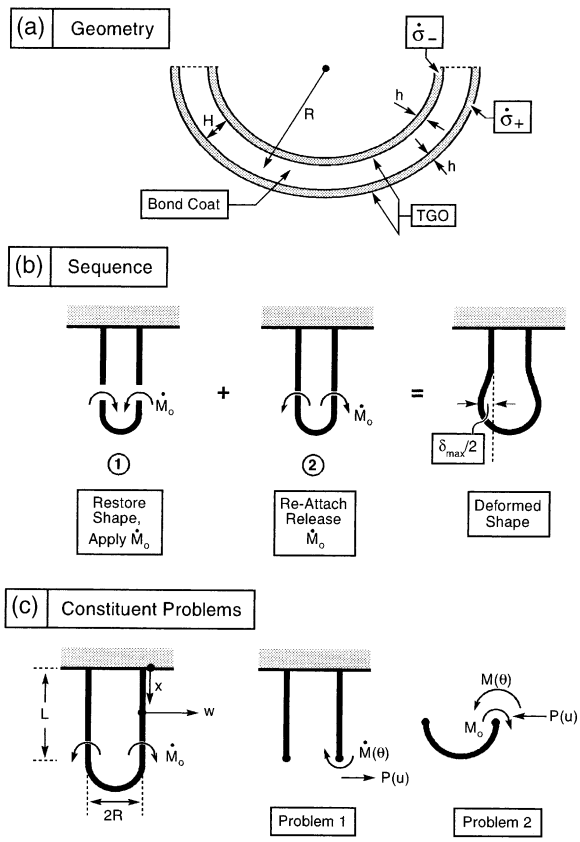

Fig. 8. Sketches of the geometry and the method used to determine the displacements and stresses that develop upon oxidation of a thin ribbon in a U-configuration.

radius of curvature, R, and curvature, $\kappa = 1/R$, is considered (Fig. 8). The width of the strip is b, σ_Y^{bc} is the flow strength of the alloy at the oxidation temperature and h_0 is a reference (initial) thickness of the TGO. Attention will be directed to the condition, $h/H \ll 1$, such that the change in curvature, $\Delta\kappa$, remains small compared to κ.

For *anion-controlled growth*, pertinent to TGO formation on FeCrAlY, an increment $\dot{h}$ of new TGO forms at the TGO/bond coat interface by consumption of bond coat, thickness $\dot{h}/m$. During the same increment, an unconstrained lateral growth strain, $\dot{\varepsilon}_g$, occurs uniformly through the TGO. If the curvature change, $\dot{\kappa}$, as well as the mid-surface strain change, $\dot{\varepsilon}_0$, is constrained to be zero (subsequently, they will be determined by superposition), the growth increment induces the following stress changes in the TGO layers (Fig. 8):

$$\dot{\sigma}_+ = \frac{m-1}{m}\bar{E}_{tgo}\kappa\dot{h} - \bar{E}_{tgo}\dot{\varepsilon}_g$$
$$\dot{\sigma}_- = -\frac{m-1}{m}\bar{E}_{tgo}\kappa\dot{h} - \bar{E}_{tgo}\dot{\varepsilon}_g \quad (2)$$

where $\bar{E}_{tgo} = E_{tgo}/(1-\nu_{tgo}^2)$ is the plane strain tensile modulus. Since the lateral growth strain is small [15], it has not been subtracted from the contribution to the TGO thickness increment. *For cation-controlled growth*, the corresponding stress changes in the TGO layers would be:

$$\dot{\sigma}_+ = -\frac{1}{m}\bar{E}_{tgo}\kappa\dot{h} - \bar{E}_{tgo}\dot{\varepsilon}_g$$
$$\dot{\sigma}_- = +\frac{1}{m}\bar{E}_{tgo}\kappa\dot{h} - \bar{E}_{tgo}\dot{\varepsilon}_g \quad (3)$$

The stresses (2) and (3) arise when the U-segment is otherwise constrained against deformation. The associated bending moment and lateral force increments are, *for anion-control:*

$$\dot{M}_0 = \frac{1}{2}(\dot{\sigma}_+ - \dot{\sigma}_-)hHb = \frac{m-1}{m}\bar{E}_{tgo}\kappa hHb\dot{h}$$
$$\dot{F}_0 = (\dot{\sigma}_+ + \dot{\sigma}_-)bh = -2\bar{E}_{tgo}hb\dot{\varepsilon}_g. \quad (4)$$

Increments of curvature, $\dot{\kappa}$, and mid-surface strain, $\dot{\varepsilon}_0$, of the composite segment are obtained by superimposing equal and opposite moment and force increments to those in (4). The TGO is taken to be elastic. The bond coat is elastic/perfectly plastic in accordance with its low creep resistance at the TGO growth temperature [19]. The additional strain increments in the segment are $\dot{\varepsilon} = -z\dot{\kappa} + \dot{\varepsilon}_0$ where z is the distance from the mid-surface. The additional stresses in the TGO are given by $\dot{\sigma} = \bar{E}_{tgo}\dot{\varepsilon}$ and those in the bond coat by $\dot{\sigma} = \bar{E}_{bc}\dot{\varepsilon}$ for $|\sigma| < \sigma_Y^{bc}$ and $\dot{\sigma} = 0$ for $|\sigma| = \sigma_Y^{bc}$.

For *anion-control*, consistent with the *outward deflection* of the U observed experimentally (Fig. 6), the equations for $\dot{\kappa}$ and $\dot{\varepsilon}_0$ obtained from imposing $\dot{M} = -\dot{M}_0$ and $\dot{F} = -\dot{F}_0$ are ($h/H \ll 1$):

$$\dot{\varepsilon}_0 + \frac{1}{2h\bar{E}_{\mathrm{tgo}}}\int_{-H/2}^{H/2}\dot{\sigma}\,\mathrm{d}z = \dot{\varepsilon}$$
$$\dot{\kappa} - \frac{2}{\bar{E}_{\mathrm{tgo}}hH^2}\int_{-H/2}^{H/2}\dot{\sigma}z\,\mathrm{d}z = -2\left(\frac{m-1}{m}\right)\kappa\frac{\dot{h}}{H}. \tag{5}$$

The integrals in (5) are the contributions from the bond coat.

Two limits are of interest. If the bond coat is elastic, (5) gives:

$$\dot{\varepsilon}_0 = \dot{\varepsilon}_{\mathrm{g}}\left[1 + \frac{H\bar{E}_{bc}}{2hE_{\mathrm{tgo}}}\right]^{-1}$$
$$\dot{\kappa} = -2\left(\frac{m-1}{m}\right)\kappa\frac{\dot{h}}{H}\left[1 + \frac{H\bar{E}_{bc}}{6hE_{\mathrm{tgo}}}\right] \tag{6}$$

If the bond coat is fully plastic (at yield though the thickness), the solution is:

$$\dot{\varepsilon}_0 = \dot{\varepsilon}_{\mathrm{g}}$$
$$\dot{\kappa} = -2\left(\frac{m-1}{m}\right)\kappa\frac{\dot{h}}{H}. \tag{7}$$

It is evident from both limits that the integrated change in curvature, $\Delta\kappa = \int\dot{\kappa}$, is small compared to the initial curvature whenever $h/H \ll 1$. Note that the lateral growth strain has no influence on the change in curvature, but it does play an important role in determining the transition between the two limits, as evident from the following numerical example.

Accordingly, the present measurement protocol has limited potential for exploring lateral strains that lead to the TGO growth stress. Its primary utility is in understanding the preference for the new TGO growth to occur at the interface relative to the free surface.

The incremental Eq. (5) have been solved numerically for the transition from elastic to fully-plastic behavior by explicitly accounting for the expanding regions of plastic yielding in the bond coat as TGO growth progresses. The incremental solution was integrated with respect to increasing h, starting from an initial stress-free state at an initial TGO thickness $h = h_0$. The resulting curvature change as a function of h is plotted in Fig. 9 for five values of $\varepsilon_Y \equiv \sigma_Y^{bc}/\bar{E}_{bc}$, including the fully plastic limit, $\varepsilon_Y^{bc} = 0$. The parameter values chosen for this plot are appropriate for the specimens used in the experiments: $\kappa_i = 1/R_i = 1/2$ mm, $H =$ 90 μm, $m =$ 2.2, and $\bar{E}_{\mathrm{tgo}}/\bar{E}_{bc} = 2$. The lateral growth strain increment is taken $\dot{\varepsilon}_{\mathrm{g}} = 0.4\dot{h}/H$ which results in $\varepsilon_{\mathrm{g}} = 0.02$ when $h/H = 0.05$. The TGO thickness at the start of the growth calculation was taken to be $h_0/H = 0.005$. The curves in Fig. 9 show that the transition from elastic to fully plastic behavior is abrupt. Moreover, the transition occurs when the TGO thickness is sufficiently large that the growth strain fully yields the bond coat core. Should this transition be explored experimentally it would be possible to extract information about the lateral growth strain. This has not been accomplished in the present experiments.

5.2. The full U-specimen

The second step of the analysis neglects the creep resistance of the bond coat. This is tanta-

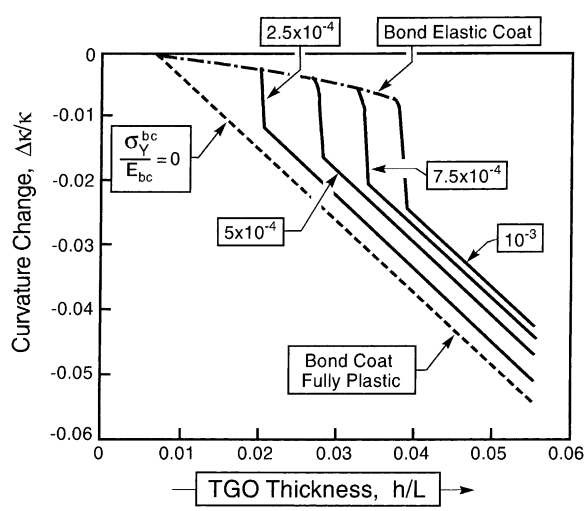

Fig. 9. The role of the yield strength of the bond coat in determining the transition from elastic to fully plastic behavior of the core, manifest in a plot of the ratio of the change in curvature to initial curvature, $\Delta\kappa/\kappa$, as a function of TGO to bond coat thickness, h/H, for an unconstrained curved segment undergoing anion controlled growth. The parameters for the system are specified in the text.

mount to assuming the incremental bending resistance of the beam derives solely from the outer elastic TGO layers: $B = \bar{E}_{tgo} h H^2 b/2$. The justification is apparent from Fig. 9. Note that, for this situation, the strains resulting from lateral growth are uncoupled from the bending and have essentially no influence on the deflection. The incremental problem for the full U is shown in Fig. 8. A moment equal but opposite in sense to that produced by the constrained growth increment, is applied at the intersections of the curved and straight segments of the U. That is, the U is notionally held at the intersection of curved segment with the straight sides and then released by applying $-\dot{M}_0$, as depicted in Fig. 8, resulting in a deflection.

The problem in Fig. 8 can be solved by standard methods in structural mechanics. Each segment is statically determinant and subject to unknown moment and transverse force at its ends. Continuity of displacement and rotation must be enforced at the intersections. (The sides are clamped at the top.) The solution for the increment in the deflection of the straight sides, $\dot{\delta}(x)$, is found to be:

$$\frac{\dot{\delta}(x)}{\dot{M}_0 R^2/B} = c_1 \ell^3 \left[\left(\frac{x}{L}\right)^2 - \frac{1}{3}\left(\frac{x}{L}\right)^3 \right] - c_2 \ell^2 \left(\frac{x}{L}\right)^2. \tag{8}$$

Here, $\ell = L/R$, and the coefficients c_1 and c_2 satisfy

$$c_1[\pi/4 + \ell^3/3] + c_2[1-\ell^2/2] = 1$$
$$c_1[1-\ell^2/2] + c_2[\pi/2 + \ell] - \pi/2.$$

Accordingly, from (4):

$$\frac{\dot{M}_0 R^2}{B} = 2\left(\frac{m-1}{m}\right) R \frac{\dot{h}}{H} \tag{9}$$

Note that the deflection increments are proportional to $\dot{h}$ and independent of h. It follows that the total deflection of one side can be integrated trivially ($h/H \ll 1$) to give:

$$\frac{\delta(x)}{R} = 2\left(\frac{m-1}{m}\right)\frac{h}{H}\left\{ c_1 \ell^3 \left[\left(\frac{x}{L}\right)^2 \frac{1}{3}\left(\frac{x}{L}\right)^3 \right] - c_2 \ell^2 \left(\frac{x}{L}\right)^2 \right\}. \tag{10}$$

Plots of normalized deflection are presented in Fig. 10 for three values of $\ell = L/R$. For the specimen to be used in the experiments, $\ell = 15$. For $l \gg 1$, the maximum displacement, δ_{max}, occurs at $x/L = 2/3$ and is given by:

$$\frac{\delta_{max}}{L} = \frac{8\pi}{27}\left(\frac{m-1}{m}\right)\frac{h}{H}. \tag{11}$$

This asymptotic expression neglects terms of relative order $1/\ell$. For $\ell = 15$, (11) overestimates the maximum deflection by 17%.

The comparisons between (11) and the measurements are presented in Fig. 7(b). As already noted, the sign affirms that the new TGO forms primarily at the TGO/alloy interface. The prediction somewhat underestimates the measurements when the volume expansion parameter, $m = 2.2$, (derived above) is used. Moreover, the largest realizable displacement (that arises when $m \to \infty$) exceeds the measurements. The implication is that a close correlation between experiment and theory requires, $m \approx 3$. This comparison shows that, subject to independent information about the volume expansion parameter, the U-test identifies the preferred location for new TGO formation in a consistent manner. Moreover, by expanding the scope of the test to different temperatures in order to examine responses around the transition from elastic to fully plastic behavior in the alloy (Fig. 9), it might be possible to assess the lateral growth strain and the associated growth stress.

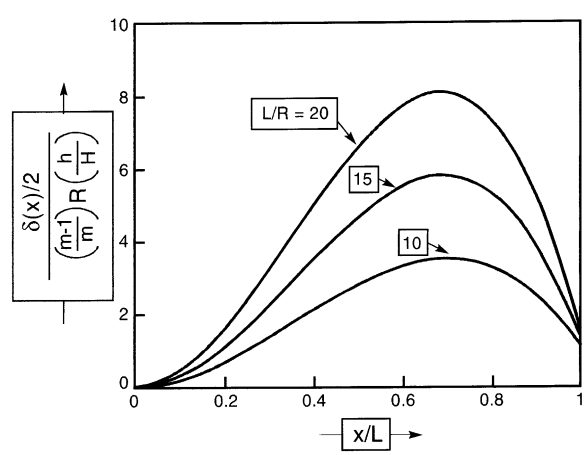

Fig. 10. Normalized deflection of the sides of the U-specimen.

6. Conclusion

An experimental probe has been designed to explore the location of the new oxide formation upon oxidation. The experiments are based on the curvature changes, $\Delta\kappa$, that occur on curved thin foils, caused by differences in strain accommodation on convex and concave surfaces. Experiments performed on thin FeCrAlY foils demonstrate a substantial increase in the radius of curvature upon oxidation, affirming that the new oxide forms primarily at the TGO/alloy interface. The situation has been analyzed by accounting for the stress relaxation that occurs in the alloy during the oxidation process. The magnitudes of the changes are found to be consistent with the experimental measurements for reasonable choices of the volume expansion parameter governing conversion of the alloy to oxide. This consis tency suggests the possibility that the scope of the tests might be expanded to explore the lateral growth strain. The model reveals that this might be achieved upon testing over a sufficient range of temperature to cause the alloy to respond to the TGO strain in a manner that changes from fully plastic (as in the present tests) to elastic/plastic or elastic.

Appendix A

Growth strain

Consider the problem where the volume rate of metal to be oxidized per unit area of interface is, $\dot{V}$. Let this volume partition between the interface, $\dot{V}_I$, and the internal grain boundaries, $\dot{V}_{GB}$, (Fig. 1) such that

$$\dot{V} = \dot{V}_I + \dot{V}_{GB}. \quad \text{(A1)}$$

Since $m-1$ is the net stress-free strain normal to the interface as the metal is converted into oxide, the thickening rate for the TGO is related to $\dot{V}_I$ by:

$$\dot{h} = (m-1)\dot{V}_I. \quad \text{(A2)}$$

If grains in the TGO are taken to be columnar and have dimension D, the volume of new oxide created on the grain boundaries causes the grains to increase in width, resulting in a growth strain. Since the metal is drawn into the boundaries and then oxidizes, from geometry (Fig. 1):

$$2hD\dot{D} = mD^2\dot{V}_{GB}. \quad \text{(A3)}$$

The growth strain-rate is related to the grain size change as:

$$\dot{\varepsilon}_g = \dot{D}/D \quad \text{(A4)}$$

whereupon, with (A3):

$$\dot{\varepsilon}_g = m\dot{V}_{GB}/2h. \quad \text{(A5)}$$

With the assumption that a fixed fraction $\Re$ of the new TGO forms internally, regardless of the TGO thickness, then from (A2) and (A5):

$$\dot{h} = (m-1)(1-\Re)\dot{V}\dot{\varepsilon}_g = m\Re\dot{V}/2h. \quad \text{(A6)}$$

Eliminating $\dot{V}$ from (A6) gives:

$$\dot{\varepsilon}_g = k\dot{h}/hk \equiv m\Re/2(m-1)(1-\Re). \quad \text{(A7)}$$

References

[1] Evans AG, Mumm DR, Hutchinson JW, Meier GH, Pettit FS. Prog. Mater. Sci. 2001;46:505–53.
[2] Stiger MJ, Yanar NM, Topping MG, Pettit FS, Meier GH. Z. Metallkd 1999;90:1069–78.
[3] Padture N. Jordan. Science 2002;296:280–4.
[4] Tolpygo VK, Clarke DR. Acta Mater. 2000;48:3283–93.
[5] Shillington EAG, Clarke DR. Acta Mater. 1999;47:1297–305.
[6] Evans AG, He MY, Hutchinson JW. Prog. Mater. Sci. 2001;46:249–71.
[7] He MY, Evans AG, Hutchinson JW. Acta Mater. 2000;48:2593–601.
[8] Karlsson AM, Evans AG. Acta Mater. 2001;49:1793–804.
[9] Mumm DR, Evans AG, Spitsberg IT. Acta Mater. 2001;49:2329–40.
[10] Gell M, Jordan E, Vaidyanathan K, McCarron K. Surf. Coat Technol. 1999;120-121:53–60.
[11] Tolpygo VK, Dryden JR, Clarke DR. Acta Mater. 2001;46:923–37.
[12] He J, Clarke DR. J. Am. Ceram. Soc. 1995;78:1347–53.
[13] Lipkin DM, Clarke DR. Oxid. Met. 1996;45:267–80.
[14] Christensen RJ, Lipkin DM, Clarke DR. Appl. Phys. Lett. 1996;69:3754–6.
[15] Clarke DR, Acta Mater., in press.
[16] Dove DB, Baldwin DH. Metall. Trans. 1974;5:1637–42.
[17] Cannon RM, Hou PY. In: Hou PY, McNallan MJ, Oltra R, Opila EJ, Shores DA, editors. Proceedings of the Symposium on High Temperature Corrosion and Materials Chemistry. Pennington, NJ: Electrochemistry Society; 1998. p. 594–607.
[18] Evans AG, Cannon RM. Mater. Sci. Forum 1989;43:243–68.
[19] Pilling NB, Bedworth RE. J. Inst. Met. 1923;29:529–82.
[20] Tolpygo VK, Clarke DR. Oxid. Met. 1998;49:187–212.
[21] Rhines FN, Wolf JS. Metall. Trans. 1970;1:1701–10.
[22] Tolpygo VK, Clarke DR. Acta Mater. 1999;47:3589–605.